

Comparing the Accumulation of Active- and Nonactive-Site Mutations in the HIV-1 Protease[†]

José C. Clemente,* Rebecca E. Moose,‡ Reena Hemrajani,‡ Lisa R. S. Whitford,‡ Lakshmanan Govindasamy,‡ Robbie Reutzel,‡ Robert McKenna,‡ Mavis Agbandje-McKenna,‡ Maureen M. Goodenow,§ and Ben M. Dunn‡

Department of Biochemistry and Molecular Biology, and Department of Pathology, Immunology, and Laboratory Medicine, University of Florida College of Medicine, Gainesville, Florida 32610

Received March 18, 2004; Revised Manuscript Received June 9, 2004

ABSTRACT: Protease inhibitor resistance still poses one of the greatest challenges in treating HIV. To better design inhibitors able to target resistant proteases, a deeper understanding is needed of the effects of accumulating mutations and the contributions of active- and nonactive-site mutations to the resistance. We have engineered a series of variants containing the nonactive-site mutations M46I and I54V and the active-site mutation I84V. These mutations were added to a protease clone (V6) isolated from a pediatric patient on ritonavir therapy. This variant possessed the ritonavir-resistance-associated mutations in the active-site (V32I and V82A) and nonactive-site mutations (K20R, L33F, M36I, L63P, A71V, and L90M). The I84V mutation had the greatest effect on decreasing catalytic efficiency, 10-fold when compared to the pretherapy clone LAI. The decrease in catalytic efficiency was partially recovered by the addition of mutations M46I and I54V. The M46I and I54V were just as effective at decreasing inhibitor binding as the I84V mutation when compared to V6 and LAI. The V6^{54/84} variant showed over 1000-fold decrease in inhibitor-binding strength to ritonavir, indinavir, and nelfinavir when compared to LAI and V6. Crystal-structure analysis of the V6^{54/84} variant bound to ritonavir and indinavir shows structural changes in the 80's loops and active site, which lead to an enlarged binding cavity when compared to pretherapy structures in the Protein Data Bank. Structural changes are also seen in the 10's and 30's loops, which suggest possible changes in the dynamics of flap opening and closing.

The development of resistance to protease inhibitors (PI)¹ during treatment of infection by the Human Immunodeficiency Virus (HIV) still poses one of the greatest challenges in the struggle to limit the virus replicative capacity. After initiation of therapy with single or multiple protease inhibitors, resistance mutations in the protease can appear within weeks. Under a constant drug selection pressure, resistant mutations continue to accumulate. It is clear that there is a correlation between the number of resistance mutations and the level of resistance and cross resistance to multiple protease inhibitors. It is of great interest to understand the level of contributions made by active- and nonactive-site mutations to the development of a high level of resistance (1–6). The HIV protease is a symmetric dimer composed of two 99-residue polypeptides (Figure 1). The dimerization region comprises the floor of the active site, which includes two catalytic aspartic acids (Asp25), one provided by each polypeptide. Unlike the human aspartic proteases that have one flap, two flaps completely cap the active site of the HIV protease. A more detailed description of HIV-1 protease

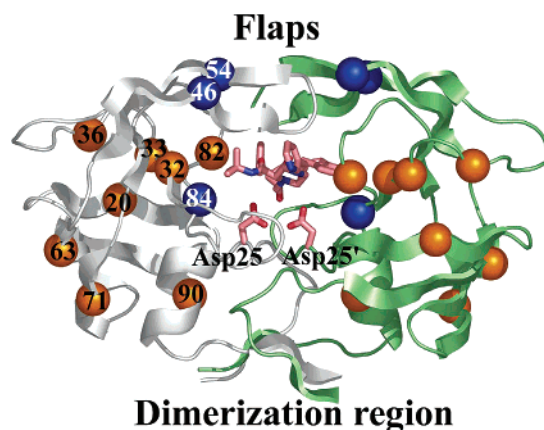


FIGURE 1: HIV-1 protease homodimer consists of two chains, A (white) and B (green). Residue changes in the V6 variant are marked by orange spheres. Mutations engineered onto the V6 variant background are shown in blue. The catalytic aspartic acids from each chain (D25 and D25') and the inhibitor indinavir are shown as red stick models in the active site. This figure was created using the V6^{54/84}–indinavir structure.

[†] This work was supported by NIH Grant AI28571 awarded to B.M.D. and M.M.G. and T32 CA09126.

* To whom correspondence should be addressed. Phone: (352) 392-3367. Fax: (352) 846-0412. E-mail: clemente@ufl.edu.

‡ Department of Biochemistry and Molecular Biology.

§ Department of Pathology, Immunology, and Laboratory Medicine.

¹ Abbreviations: IPTG, isopropylthio- β -galactopyranoside; dTT, dithiothreitol; Nph, *p*-NO₂-L-phenylalanine; nL, L-norLeucine; protease inhibitor, PI.

structure, inhibitor binding, and resistance can be found in reviews by Wlodawer and Gustchina, Tomasselli and Heinrichson, and Dunn (7–9).

In this study, we analyze the effect of adding the nonactive-site mutations M46I and I54V and the active-site mutation I84V to a post-ritonavir therapy protease variant (V6) already containing PI-resistance-associated mutations

Table 1: Variants and Residue Changes^a

variants	mutations
LAI	
1HXW	S37N
1HSG	
V6	K20R V32I L33F M36I L63P A71V V82A L90M
V6 ⁴⁶	
V6 ⁵⁴	V6 + I54V
V6 ⁸⁴	V6 + I84V
V6 ^{46/84}	V6 + M46I I84V
V6 ^{54/84}	V6 + I54V I84V
V6 ^{46/54/84}	V6 + M46I I54V I84V

^a Mutations found in the active site are in bold font.

at residues 20, 32, 33, 36, 63, 71, 82, and 90 (Figure 1 and Table 1). Mutated residues in variant V6 compared to LAI (wild type) are shown in Table 1. Molla et al. showed that mutations in the protease gene during ritonavir therapy occurred in an ordered fashion (10). Mutation V82A was associated with the initial loss of antiviral activity. Subsequently, the following mutations were observed most frequently: I54V, A71V, and M36I. Later, proteases containing mutations I84V, K20R, M46I, L33F, and L90M appeared. The mutation I84V has been seen in patients receiving ritonavir, indinavir, amprenavir, and saquinavir therapy and tends to develop in combination with L90M to provided a high level of clinical resistance (11, 12). Mutations at position 54, I54L/T/M, and most frequently I54V, have been reported in response to ritonavir, indinavir, amprenavir, saquinavir, and lopinavir (10, 13, 14). The mutation M46I has been observed in response to therapy with ritonavir, amprenavir, indinavir, and nelfinavir (10, 13, 14).

This study analyzed the effect of accumulating two commonly observed nonactive-site mutations (M46I and I54V) on inhibitor binding and substrate catalysis. It also aimed to study the effect of adding the active-site mutation I84V to address the level of biochemical resistance, cross resistance, and individual contribution to resistance between active- and nonactive-site mutations. Finally, we addressed the structural changes in the most resistant protease by determining its crystal structure in complex with ritonavir and indinavir. These experiments showed the level of resistance and cross resistance incurred by a large number of mutations commonly seen in response to ritonavir therapy.

EXPERIMENTAL PROCEDURES

Mutagenesis and Expression of Protease. A complete description of the cloning, expression, and purification procedures can be found in Ido et al. and Goodenow et al. (15, 16). In brief, the HIV-1 PR DNA for all of the HIV LAI variants was subcloned into the pET23a expression vector (Novagen) (17). The construct was transformed into the *Escherichia coli* strain BL21 Star DE3 PlyS from Invitrogen. All other constructs were subcloned into the pET11a vector (Novagen) and transformed into the *E. coli* strain JM109 DE3. The introduction of all mutations onto the V6 background was done using the QuikChange Mutagenesis Kit from Stratagene. Protease expression was initiated when OD₆₀₀ reached 0.6 by addition of 1 mM IPTG to a culture grown at 37 °C in M9 media (6.8 g of Na₂HPO₄, 3 g of KH₂PO₄, 0.5 g of NaCl, 1 g of NH₄SO₄, and 5 g of Casamino Acids were autoclaved together in 987 mL

of H₂O, and then 1 mL of 0.1 M CaCl₂, 2 mL of 1.0 M MgSO₄, 10 mL of 20% glucose, and 50 µg/L of ampicillin were added). After 3 h, cells were harvested by centrifugation at 16000g for 5 min and resuspended in TN buffer (0.05 M Tris, 0.15 M NaCl, and 0.001 M MgCl₂ at pH 7.4). Inclusion bodies containing the protease were isolated by centrifugation through a 27% sucrose cushion. The inclusion bodies were solubilized in 8 M urea, and the protease was refolded by dialysis against 0.05 M sodium phosphate buffer (0.05 M Na₂HPO₄, 0.005 M EDTA, 0.3 M NaCl, and 0.001 M dTT at pH 7.3). The protease was purified through ammonium sulfate precipitation and gel-filtration chromatography using a Superdex 75 16/60 column from Amersham Pharmacia, attached to an FPLC LCC 500 Plus, also from Amersham Pharmacia. The protease was eluted using potassium phosphate buffer (50 mM K₂HPO₄, 2 mM EDTA, 150 mM NaCl, 2 mM dTT, 5% glycerol, and 5% 2-propanol at pH 7.3).

Protease Activity and Inhibitor Constants. The Michaelis–Menten constants k_{cat} , K_m , and k_{cat}/K_m and K_i values were determined for each variant as previously described (18). The chromogenic substrate K-A-R-V-L*Nph-E-A-nL-G, which mimics the CA-p2 cleavage site, was used to determine the catalytic activity of each variant at 37 °C in sodium acetate buffer (0.05 M NaOAc, 0.15 M NaCl, 0.002 M EDTA, and 0.001 M dTT at pH 4.7). K_i values for all inhibitors were determined under the same conditions. Cleavage of the substrate was monitored using a Hewlett–Packard 8452A spectrophotometer equipped with a 7-cell sample handling system as described by Dunn et al. (19). The inhibition constants K_i were determined by monitoring the inhibition of hydrolysis of the chromogenic substrate as described by Bhatt et al. (20).

Crystallization of Protein–Inhibitor Complexes. Inhibitors were dissolved in 100% DMSO and mixed with the protein in a molar ratio of 10:1. The enzyme concentration used was 3 mg/mL in 50 mM sodium acetate at pH 4.7. The final concentration of DMSO was 10%. The inhibitor–protein mixture was combined with the reservoir solution in a 1:1 (v/v) ratio to set up hanging drops of 4 µL at room temperature. The reservoir solution contained 1.5 M ammonium sulfate and 20 mM sodium acetate at pH 6.0 and 4.5 for the ritonavir and indinavir complexes, respectively. Rod-shaped crystals appeared overnight and grew to full size in a week.

Data Collection, Structure Determination, and Refinement. X-ray diffraction images for the ritonavir and indinavir complexes were collected at room temperature and 100 °K, respectively, using an R-Axis IV++ image plate system with Osmic mirrors and a Rigaku HU-H3R Cu rotating anode operating at 50 kV and 100 mA. Each data set was collected from a single crystal. The indinavir complex crystal was dipped in a cryoprotectant solution (30% glycerol in reservoir solution) prior to data collection. The data were indexed, scaled, and reduced using DENZO and SCALEPACK (21). Both complexes were crystallized in the hexagonal $P6_1$ space group.

Initial phases were calculated by the molecular replacement method, employing the coordinates of the HIV-1 protease–ritonavir structure (PDB entry 1HXW) as a search model after removing the inhibitor and water molecules. Standard methods of structure refinement were then employed using programs in CNS Suite (22). Difference electron density

Table 2: X-ray Crystallography Data Collection Statistics

	ritonavir	indinavir
wavelength (Å)	1.5418	1.5418
resolution range (Å)	20–2.5	20–1.9
space group	$P6_1$	$P6_1$
unit-cell parameters a, c (Å)	62.1, 84.7	61.6, 84.1
number of reflections	87 389	148 116
number of unique reflections	6434	13 795
overall completeness (%)	97.8 (89.9)	96.6 (80.6)
average I/σ	4.7	5
R_{sym}^a (%)	13.2 (51.1)	5.6 (24.6)
PDB ID	1SGU	1SH9
Refinement statistics		
R_{work}^b (%)	21.1 (26.2)	21.9 (27.3)
R_{free}^c (%)	27.5 (36.2)	26.3 (31.1)
rmsd bond length (Å)	0.01	0.01
rmsd bond angles (deg)	1.3	1.5
average B factor (Å ²)	24.28	22.41
main/side chains	22.29/25.57	20.11/23.72
inhibitor atoms	34.52	30.34
water molecules	27.64	27.75
Ramachandran plot quality		
most favored (%)	93.5	93.6
additionally allowed (%)	5.8	6.4
generally allowed (%)	0.6	0
disallowed (%)	0	0

^a $R_{\text{sym}} = \sum_{hkl} (|I(hkl)| - \langle I(hkl) \rangle) / \langle I(hkl) \rangle \times 100$ where $I_i(hkl)$ is the i th observation of the intensity of a reflection with indices h , k , and l and $\langle I(hkl) \rangle$ is the average intensity of all symmetry equivalent measurements of that reflections. ^b $R_{\text{work}} = \sum_{hkl} (F_{\text{obs}}(hkl) - F_{\text{calc}}(hkl)) / F_{\text{obs}}(hkl) \times 100$, where $F_{\text{obs}}(hkl)$ and $F_{\text{calc}}(hkl)$ are the observed and calculated structure factor amplitudes, respectively. ^c R_{free} was calculated using 5% of data excluded during the refinement process. In parenthesis is the highest resolution shell.

maps with coefficients $2F_o - F_c$ and $F_o - F_c$ were used to guide manual fitting of the models in the molecular graphics program O7 (23). Amino acid differences were observed in the electron density (compared to 1HXW) and were replaced according to the V6^{54/84} sequence. Water molecules were added into the model using a density set at 2σ . In the final stage of the refinement, the inhibitors were modeled into the active site. During model building and refinement, 5% of the data was reserved for cross validation to monitor the refinement progress. Details of the data collection and refinement statistics are shown in Table 2. The atomic coordinates have been deposited in the Protein Data Bank: 1SGU and 1SH9 for indinavir and ritonavir structures, respectively.

Figures 1–4 and 6–8 were generated using the PyMOL Molecular Graphics System (24). The separated surfaces were generated using the Molcad module in Sybyl 6.9 (25, 26). The separated surfaces were calculated between the van der Waals surfaces of all atoms and are defined by a set of points halfway between the shortest distance separating the inhibitor and the enzyme. Grid width was set to 0.4 Å, and virtual sphere radius was set to 4.0 Å. Structural alignments of backbone atoms were done using the Biopolymer module in Sybyl 6.9.

RESULTS

Kinetic Analysis. The K_m , k_{cat} , and k_{cat}/K_m parameters were determined for LAI, a pretherapy isolated protease (wild type), and seven variants, V6, V6⁴⁶, V6⁵⁴, V6⁸⁴, V6^{46/84}, V6^{54/84}, and V6^{46/54/84}, using a synthetic substrate that mimics the CA-p2 site of Gag (Table 3). The V6, V6⁴⁶, V6⁵⁴, and

Table 3: Michaelis–Menten Constants^a

variants	K_m (μM)	k_{cat} (sec ^{−1})	k_{cat}/K_m (μM ^{−1} sec ^{−1})
LAI	18 ± 2	21 ± 2	1.2 ± 0.2
V6	47 ± 5 (3)	27 ± 2 (0.8)	0.58 ± 0.07 (1)
V6 ⁴⁶	27 ± 4 (2)	12 ± 1 (2)	0.43 ± 0.07 (3)
V6 ⁵⁴	49 ± 7 (3)	17 ± 1 (1)	0.34 ± 0.06 (4)
V6 ⁸⁴	40 ± 5 (2)	4.3 ± 0.6 (5)	0.11 ± 0.02 (10)
V6 ^{46/84}	43 ± 4 (2)	9.9 ± 0.9 (2)	0.23 ± 0.03 (5)
V6 ^{54/84}	48 ± 8 (3)	7.1 ± 0.9 (3)	0.15 ± 0.02 (8)
V6 ^{46/54/84}	33 ± 4 (2)	6.8 ± 0.9 (3)	0.21 ± 0.02 (5)

^a Fold change from LAI are in parenthesis.

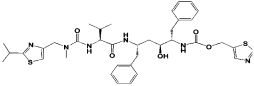
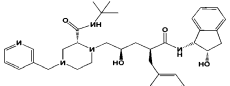
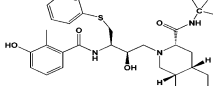
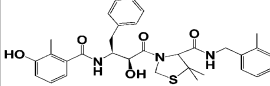
V6⁸⁴ variants all experienced a decrease in k_{cat}/K_m of 2-, 2-, 3-, and 10-fold, respectively, when compared to LAI (Table 2). Variants V6^{46/84}, V6^{54/84}, and V6^{46/54/84} showed a decrease in k_{cat}/K_m of 5-, 8-, and 6-fold, respectively, when compared to LAI.

Dissociation Constants. The K_i values for the wild-type enzyme with all of the inhibitors tested were subnanomolar to low nanomolar in agreement with other studies (Table 4) (5, 27–29). The V6 variant showed a large decrease in susceptibility to ritonavir. This was not surprising because this variant was isolated from a pediatric patient on ritonavir therapy. A 43- and 22-fold increase in K_i was also seen for nelfinavir and indinavir, respectively. The V6 variant only offered a small level of biochemical cross resistance to AG1776, when compared to indinavir, nelfinavir, and ritonavir, even though V6 contains various mutations commonly seen in response to multiple inhibitors, specifically the key mutations V82A and L90M (10–13, 30–33).

The addition of mutation M46I, which is seen in response to each inhibitor tested, decreased the potency of all of the inhibitors, with indinavir showing the lowest potency with a 630-fold increase in the K_i value followed by nelfinavir (96-fold), ritonavir (90-fold), and AG1776 (23-fold). It should be noted that AG1776 still bound with a subnanomolar dissociation constant. The addition of mutation I54V to V6 had the greatest effect on the binding of ritonavir and indinavir with a 155- and 127-fold decrease in affinity, respectively. The V6⁵⁴ variant showed a lesser effect on nelfinavir and AG1776 with an 18- and 8-fold increase in the K_i value, respectively. Variant V6⁸⁴ showed a greater decrease in inhibitor susceptibility (235-fold) to ritonavir than did V6⁴⁶ and V6⁵⁴. To our surprise, the addition of mutation I84V decreased the binding affinity of indinavir to a lesser extent than M46I and I54V, 540- and 34-fold less, respectively, and the affinity of nelfinavir was 96-fold less than that of the mutation M46I. Of the single mutations added to V6, I84V showed the greatest effect on the binding of AG1776 with a 25-fold increase in the K_i value.

The double mutant V6^{46/84} further decreased the binding of ritonavir when compared to V6, V6⁴⁶, V6⁵⁴, and V6⁸⁴ from 250- to 450-fold. Although this variant showed a decrease in susceptibility to indinavir when compared to V6 (20-fold), a greater decrease was seen for variants V6⁴⁶ (630-fold) and V6⁵⁴ (130-fold). Addition of mutations M46I and I84V to V6 lessened the affinity of nelfinavir by 19-fold when compared to that of LAI but was less than what was seen with the single mutants. Variant V6^{46/84} also showed a large decrease in susceptibility to AG1776 (104-fold) when compared to any of the variants discussed thus far. Although a large fold decrease in inhibitor susceptibility was seen with previously

Table 4: Dissociation Constants (K_i)^a

Variants	Inhibitor K_i (nM)			
	Ritonavir	Indinavir	Nelfinavir	AG1776
				
LAI	0.7 ± 0.1	3.1 ± 0.1	1.2 ± 0.2	0.021 ± 0.004
V6	30 ± 2 (42)	69 ± 8 (22)	17 ± 3 (14)	0.04 ± 0.01 (2)
V6 ⁴⁶	65 ± 8 (92)	1963 ± 242 (632)	116 ± 14 (96)	0.5 ± 0.1 (23)
V6 ⁵⁴	109 ± 9 (155)	398 ± 77 (127)	23 ± 2 (18)	0.19 ± 0.05 (8)
V6 ⁸⁴	165 ± 26 (235)	289 ± 28 (93)	24 ± 3 (19)	0.55 ± 0.02 (25)
V6 ^{46/84}	345 ± 40 (492)	62 ± 5 (19)	52 ± 2 (42)	2.2 ± 0.3 (104)
V6 ^{54/84}	932 ± 83 (1330)	4235 ± 506 (1359)	1259 ± 117 (1048)	9.4 ± 0.3 (447)
V6 ^{46/54/84}	624 ± 76 (890)	2914 ± 463 (939)	563 ± 65 (468)	5.6 ± 0.2 (266)

^a Fold change from LAI are in parenthesis.

discussed variants, this is the first variant to show a K_i value above subnanomolar for AG1776. Variant V6^{54/84} exhibits the least susceptibility to inhibition by all of the inhibitors tested compared to that of LAI. Ritonavir, indinavir, and nelfinavir all experience a greater than 1000-fold decrease in inhibition strength compared to that of LAI and V6. Inhibitor AG1776 showed a 450-fold decrease in inhibition strength compared to that of both LAI and V6. The triple mutant V6^{46/54/84} also showed a large decrease in inhibitor susceptibility to all of the inhibitors tested. This variant experienced an 890-, 939-, 468-, and 266-fold decrease in the K_i value to ritonavir, indinavir, nelfinavir, and AG1776, respectively.

Structural Analysis. To further understand the large increase in K_i values caused by the mutations analyzed in this study, we crystallized the variant V6^{54/84}, which showed the greatest decrease in inhibitor-binding strength to all inhibitors tested, in complex with ritonavir and indinavir, and solved the structures at 2.5 Å and 1.9 Å resolution, respectively (Figure 2). The structural overlaps of the wild-type ritonavir (PDB 1HXW) and indinavir (PDB 1HSQ) complexes and V6^{54/84} in complex with ritonavir and indinavir are shown in Figure 3. Sequence differences between the wild-type structure proteases and LAI are shown in Table 1.

V6^{54/84}–Indinavir Structure. Structural alignment of Cα atoms of V6^{54/84}–indinavir and the wild-type protease–indinavir structure shows large structural changes in the 10's (residues 14–20), 30's (residues 30–40), 60's (residues 63–73), and 80's (residue 78–85) loops (Figure 3A). The average distances between equivalent Cα atoms over the 99 residues in chains A and B of the two structures are 0.57 and 0.56 Å, respectively. The average Cα separation between the two structures and the residue number at peak distance for the loops listed above are shown in Table 5. Although the loops in both chains of the homodimer show an increase in the separation of equivalent Cα atoms, the magnitude is asymmetric. This is most likely an effect from the asymmetric inhibitor bound in the active site.

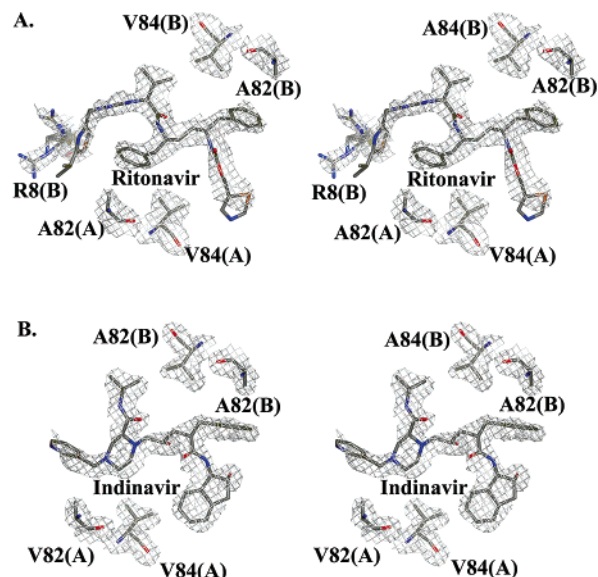


FIGURE 2: Stereoview of $2F_o - F_c$ electron density of (A) ritonavir and (B) indinavir in the active site of variant V6^{54/84}. Residue 8 in chain B of the ritonavir complex is shown occupying two conformations. Residues 82 and 84 in chain A and B are shown for both structures. Electron density is drawn to the 1σ level.

The V6^{54/84} variant contains three mutations in the active site, V32I, V82A, and I84V, and occupies the S2/S2' (32) and S1/S1' (82 and 84) pockets. These pockets interact with the core of the inhibitor. The interaction of indinavir with the active-site residues of both the wild-type and V6^{54/84} enzyme was compared using LIGPLOT (57). Shown in Figure 4 are the hydrophobic interactions with residues 32, 82, and 84 and all hydrogen bonds between the inhibitor and the enzyme. Indinavir makes no hydrophobic contact with residues Ile32(A), Ala82(A), and Val84(A) and (B) in the V6^{54/84} structure. There are two hydrophobic points of contact made between Ile32(B) and the aminoindanol in the P2' position of indinavir. Three hydrophobic points of contact are made between A82(B) and the P1' phenyl ring of indinavir. When compared to the wild-type structure, this

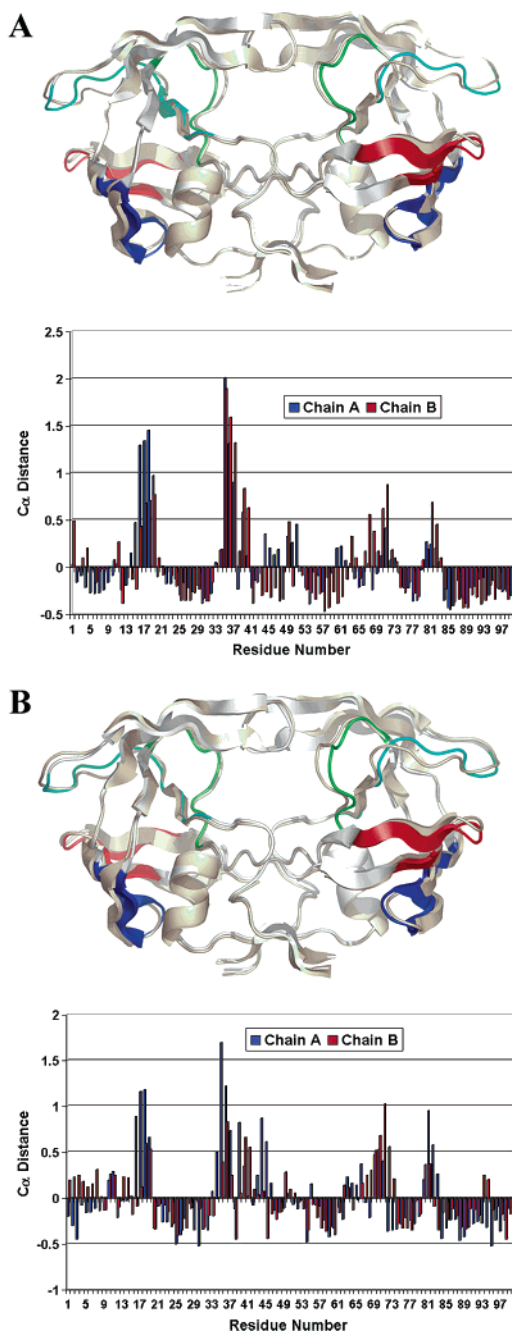


FIGURE 3: Ribbon representation of a C α overlap of (A) 1HSG (white) and V6^{54/84}–indinavir (beige) and (B) 1HXW (white) and V6^{54/84}–ritonavir (beige) structures. The 10's, 30's, 60's, and 80's loops are colored blue, aqua, red, and green, respectively, in the mutant structures. Below each structure is a bar-graph representation of the C α distances between the wild-type structure and V6^{54/84} for chain A (blue) and chain B (red). These graphs were created by subtracting the average C α separation for each chain from the C α distance of each residue in the corresponding chain.

equates to a loss of four hydrophobic points of contact encompassing residues 32(A), 82(A), and 84(B). Indinavir establishes four direct and four water-mediated hydrogen bonds with active-site residues. When compared to the wild-type structure, one direct and one water-mediated hydrogen bond are lost. Generation of a separated surface showed a volume of 1266 Å³ and an area of 1001 Å² of interaction between the enzyme and inhibitor (Figure 5A). When compared to the wild-type structure there is an increase in the volume and area of 230 Å³ and 131 Å², respectively, in

Table 5: C α Distances for the 10's, 30's, 60's, and 80's Loops between the V6^{54/84} and Wild-Type Structures

V654/84–Indinavir and 1HSG		
loop ^a	C α (Å) ^b	peak distance ^c
Chain A		
10 (14–20)	0.8	1.4 (18)
30 (30–40)	0.3	1.9 (35)
60 (63–73)	0	0.4 (71)
80 (78–85)	0	0.3 (80)
Chain B		
10 (14–20)	0.3	0.7 (19)
30 (30–40)	0.5	2.0 (35)
60 (63–73)	0.3	0.9 (71)
80 (78–85)	0.1	0.7 (81)
V6 ^{54/84} –Ritonavir and 1HXW		
Chain A		
10 (14–20)	0.1	0.6 (18)
30 (30–40)	0.1	0.8 (36)
60 (63–73)	0.3	1.0 (71)
80 (78–85)	0	0.4 (80)
Chain B		
10 (14–20)	0.5	1.2 (17 and 18)
30 (30–40)	0.4	1.7 (35)
60 (63–73)	0.1	0.5 (69 and 70)
80 (78–85)	0.1	1.0 (81)

^a Loops in chain A and B. In parenthesis are the residue numbers, which makeup that loop. ^b Average C α distance for each loop. ^c Maximum C α distance for each loop and residue number.

the separated surface of interaction. The increase in the volume and area can be mapped to the S1', S2, and S2' sites.

V6^{54/84}–Ritonavir Structure. The V6^{54/84}–ritonavir structure also shows structural changes in the 10's, 30's, 60's, and 80's loops when compared to the wild-type complex of ritonavir (Figure 3B). The average distances between equivalent C α atoms and the residue number at peak distance for the loops listed above are shown in Table 5. The average C α separations between the two structures over the 99 residues in chains A and B are 0.64 and 0.52 Å, respectively. As with the indinavir structure, there is an asymmetry in the C α distance variations in each loop between the two chains. Again, this is most likely an effect of the asymmetric inhibitor bound in the active site.

The interactions of ritonavir with the active-site residues 32, 82, and 84 of the V6^{54/84} enzyme were compared using LIGPLOT. Shown in Figure 4 are hydrophobic interactions and all hydrogen bonds between the inhibitor and the enzyme. Ritonavir in the V6^{54/84} variant makes no hydrophobic contacts with residues Ala82(A) and (B) and Val84(A) and (B). Two hydrophobic points of contact are made between the Ile32(A) residue and the Val side chain of ritonavir in the S2 pocket. One hydrophobic point of contact is made between the Ile32(B) residue and the methoxycarbonyl group of ritonavir occupying the S2' pocket. When compared to the wild-type structure, there is a total loss of six hydrophobic points of contact with residues 82(A) and (B) and 84(A). Ritonavir establishes four direct and one water-mediated hydrogen bond with active-site residues. When compared to the 1HXW structure, two direct and one water-mediated hydrogen bond are lost. Generation of a separated surface showed a volume of 1341 Å³ and an area of 985 Å² of interaction between the enzyme and inhibitor (Figure 5B). When compared to the wild-type structure, there

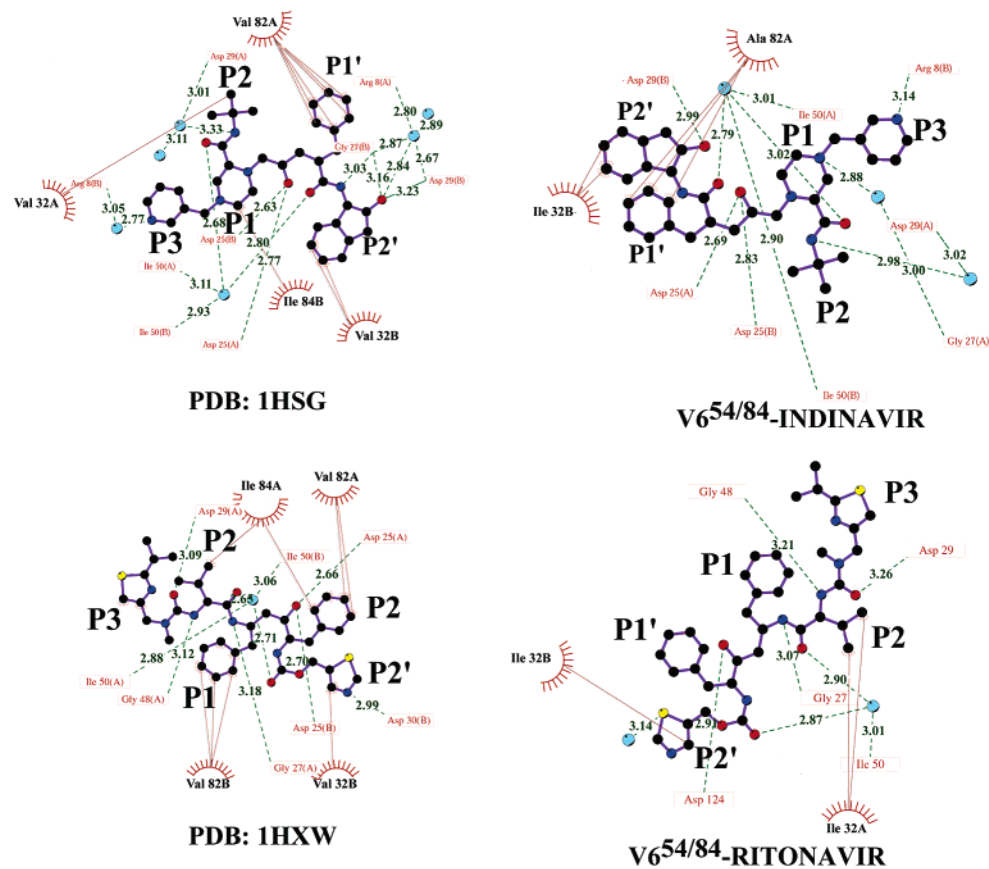


FIGURE 4: LIGPLOT representation of hydrophobic interactions between the inhibitors and residues 32, 82, and 84 and hydrogen-bonding interactions in the wild-type (left) and V6^{54/84} (right) protease.

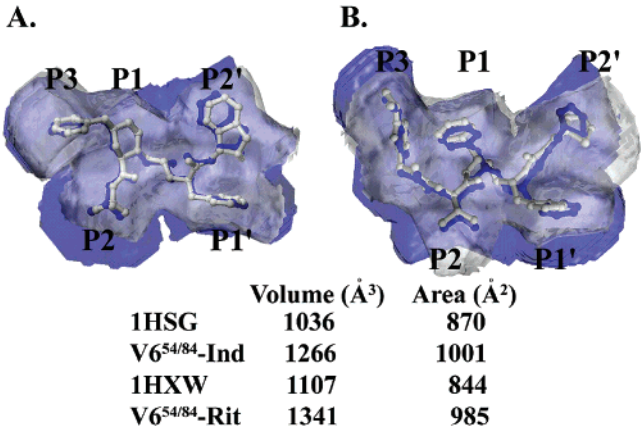


FIGURE 5: (A) Separated surface overlap of V6^{54/84} in complex with indinavir (blue) and 1HSG (white). An increase in the separated surface area and volume can be seen for the P1, P2, and P2' groups. (B) Separated surface overlap of V6^{54/84} in complex with ritonavir (blue) and 1HXW (white). An increase in the separated surface area and volume can be seen for all side groups except P1.

is an increase in the volume and area of 234 Å³ and 114 Å², respectively, in the separated surface of interaction. The increase in the volume and area can be mapped to the S1', S2, S2', and S3 sites.

DISCUSSION

The initial resistant variant on which we based our study, V6, was isolated from a pediatric patient while on ritonavir therapy and contains various mutations commonly seen in response to ritonavir (Table 1). We then added mutations in

the flaps (M46I and I54V) and active site (I84V) to assess the effect of accumulating nonactive- and active-site mutations. We analyzed the catalytic efficiency of all variants using a chromogenic substrate that mimics the CA-p2 cleavage site of Gag-Pol. Processing at this site has been shown to be a key regulatory event in the ordered cleavage of Gag-Pol generating mature infectious viruses (34, 35). The V6 variant when compared to LAI shows a 50% decrease in catalytic efficiency (k_{cat}/K_m) mainly because of a 3-fold increase in K_m . Chen et al. reported a mutant protease carrying mutations M46I/L63P, which was catalytically more efficient than wild-type enzyme, while a variant carrying mutations V82T/I84V had very poor catalytic activity (36). This would suggest that mutations at positions 46 and 63 should compensate for a decrease in catalytic efficiency because of mutations at positions 82 and 84. The variants we analyzed in this study contain, in addition to M46I and L63P, M36I and A71V mutations also thought to compensate for catalytically deleterious mutations (37, 38). The active-site mutation I84V was the only single mutation when added to V6 that caused a significant decrease in k_{cat}/K_m (10-fold). The addition of mutations M46I and I54V to V6 also decreased the catalytic efficiency of the protease when compared to V6 by 2- and 3-fold, respectively. Addition of mutations M46I and/or I54V to the V6⁸⁴ variant improved catalytic activity when compared to that of V6⁸⁴ by up to 5-fold for variant V6^{46/84}. Pazhanisamy et al. showed that a protease carrying M46I was catalytically less efficient than the wild-type protease with the substrate used in this study, but when comparing V6^{46/84}, V6^{54/84}, and V6^{46/54/84}, it appears that the M46I mutation provides a greater improvement in

catalytic efficiency than the I54V substitution (39). Surprisingly, the addition of the mutations M46I and/or I54V did not improve the catalytic efficiency of the V6 variant, which contains the active-site mutations V32I and V82A and the nonactive-site mutations L63P, M36I, and A71V. Protease sequences from additional viruses isolated at 28 and 40 weeks show the presence of the M46I or I54V mutations (data not shown). This suggests that the decrease in catalytic efficiency offered by the M46I and I54V mutations is acceptable for virus replication and is selected for decreasing the inhibitor binding. Also, improvements in catalytic activity are a product not of individual residues but of residue combinations.

We analyzed the inhibition of all variants with the three clinically used inhibitors ritonavir, indinavir, and nelfinavir. We also tested the inhibition of these variants by the inhibitor AG1776, which is an allophenylnorstatine-based lead compound that has shown strong inhibition of HIV-1-resistant variants (40). The V6 variant showed a 42-fold decrease in inhibition by ritonavir. This was expected because V6 was isolated from a patient receiving ritonavir. The V6 variant also showed cross resistance to nelfinavir and indinavir but maintained susceptibility to AG1776. V6 contains six mutations (K20R, V32I, M36I, L63P, A71V, and V82A) commonly seen in response to indinavir therapy, which highly overlap with mutations commonly seen to ritonavir. V6 carries three mutations (M36I, A71V, and V82A) commonly seen in response to nelfinavir therapy. We previously demonstrated the cooperative effect of M36I and A71V with the active-site mutation D30N to provide for the high level of resistance to nelfinavir (18). The combination of mutations in V6 does not provide for a high level of resistance to AG1776. The most frequently seen mutations in vitro in response to AG1776 include M46I, I47V, and I84V and less frequently, V32I and V82I (41). The susceptibility of V6 to inhibition by AG1776 might be due to the presence of only a single low occurring specific mutation, V32I, seen in vitro in response to this inhibitor.

The addition of mutation M46I (V6⁴⁶) had its greatest effect on the binding of indinavir with a 630-fold increase in K_i when compared to that of LAI and 28-fold for V6. The V6⁴⁶ enzyme carries two major mutations (V82A and M46I) commonly seen in response to indinavir. The M46I mutation also decreased the binding affinity for the three other inhibitors tested but not to the same degree. The M46I mutation is not considered a major mutation for ritonavir or nelfinavir and caused only a ~2-fold increase in the K_i value for both inhibitors when compared to that of V6. The M46I mutation is considered a major mutation for AG1776 and caused a ~10-fold increase in K_i for this inhibitor. It should be noted that AG1776 still binds with a subnanomolar K_i value. The I54V mutation is not considered a major mutation against any of the inhibitors tested, and it is not a mutation associated with nelfinavir resistance. This mutation is, however, highly associated with the V82A mutation, which has been associated with resistance to all clinically used inhibitors (42, 43). The addition of mutation I54V (V6⁵⁴) generated an enzyme less susceptible to ritonavir (~4-fold), indinavir (~80-fold), and AG1776 (~5-fold) and an enzyme more susceptible to nelfinavir (~2-fold) when compared to that of V6.

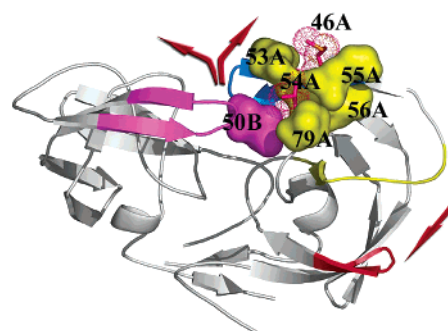


FIGURE 6: Mutations at residues 46 and 54 destabilize the flaps. The homodimer is shown as a white ribbon C α trace. The flaps of chain A and B are colored magenta and blue, respectively. The 10 and 30 loops of chain A are colored red and yellow, respectively. Residues 53, 55, 56, 79, and 47 in chain A are shown as a yellow van der Waals surface. Residue 50 in chain B is shown as a magenta van der Waals surface. Residues 46 and 54 are shown as red sticks and a van der Waals dot surface. The red shows the movement of the 30's loops and the opening of the flaps. This figure was created using PDB 1HSG.

Both the M46 and I54 residues are found in the flaps of the protease. Ohtaka et al. previously demonstrated cooperative interactions between M46I and I54V and the active-site V82A and I84V mutations to provide for a high level of cross resistance (44). The M46 residue occupies a hydrophobic groove occupied by residues Lys55 and Phe53 in the juxtaposed flap β strand (Figure 6). The I54V mutation sits in a hydrophobic pocket formed by residues Pro79, Ile47, and Val56 in the same chain and residue Ile50 in the flap of the opposite chain. It is clear that residue Ile54 is involved in stabilizing the closed conformation of the flaps and would play a role in the dynamics of flap opening and closing. The M46I mutation juxtaposed to residue 54 and interacting with the residues on either side of 54 is potentially contributing to changes in the interactions between residue 54 and the surrounding residues previously discussed. Examination of the structure (PDB 1C6Y) of a complex of an HIV-1 protease, containing nine mutations including M46I and I54V, with indinavir shows a major change in the position of the 80's loop of chain B but little difference in the closed conformation of the flaps when compared to that of the wild type (45). The structure of variant V6^{54/84} in complex with indinavir and ritonavir also shows changes in the conformation of the 80's loops and little change in the closed conformation of the flaps. This suggests that the effects of mutations M46I and I54V are not affecting the final bound conformation but might be affecting the mechanics of the flaps opening and closing or the stability of the opened or closed conformation.

The addition of the active-site mutation I84V to the V6 variant was not on average as deleterious as adding the nonactive-site mutations M46I or I54V. Combination of I54V with I84V generated the most inhibition insensitive enzyme (V6^{54/84}) having greater than a 1000-fold increase in K_i to all three clinically used inhibitors tested and greater than 450-fold increase for that of AG1776. The variant carrying the triple mutation combination showed the second highest decrease in susceptibility to all of the inhibitors tested but showed higher catalytic activity than the V6^{54/84} and V6⁸⁴ variants. The accumulation of these mutations provides for an enzyme that is highly cross-resistant and maintains

sufficient catalytic activity for virus viability, >5% of wild-type activity (46–48).

The inhibitor AG1776 shows a large fold increase in K_i to the double and triple mutants when compared to that of the wild type, but when compared to the clinically used inhibitors, it shows an up to 450-fold greater potency. A recent paper by Vega et al. characterizing AG1776 (also known as KNI-764 and JE-2147) by calorimetry and X-ray crystallography shows that its ability to inhibit resistant variants is a product of enthalpy/entropy compensation and structural adaptability (49).

The crystal structure of V6^{54/84} in complex with indinavir and ritonavir shows significant structural changes to the regions containing the described mutations compared to the equivalent areas in the wild-type structures (Figure 3). In both structures, changes in the conformation of the 80's loops are seen. The 30's and 80's loops have previously been shown to affect substrate specificity (45, 50, 51). Unlike the structure of a mutant protease complexed with indinavir reported by Munshi et al., where the 80' loop in chain B moves away from the active site and the P3 group of the inhibitor adopts an alternate conformation, in our structure of ritonavir and indinavir, the 80's loops have moved closer to the active site and the inhibitors display a similar binding mode to that of the wild-type structure. Although the 80's loops have moved closer to the inhibitor, analysis of the active site shows an enlarged binding cleft (Figure 5). The V82A and I84V mutations create expanded S1–S3 and S1'–S3' pockets (Figures 4 and 5). Unexpectedly, the V32I mutation also created larger S2 and S2' pockets. The increase in surface area separating the interface between the inhibitor and the enzyme predicts a decrease in the level of interactions between them. A comparison of the wild-type and V6^{54/84} structures shows a loss of hydrophobic contact with residues 32, 82, and 84, in both chains and a loss of hydrogen-bonding interactions (Figure 4). Instability in the bound inhibitor can also be seen in the P3 group of both complexes, which is defined by poor density (Figure 2). Residue 82 is located between the S1 and S3 subsites and can interact with both the P1 and P3 groups of the inhibitors. Residue 82 and 8 sandwich the P3 thiazolyl group of ritonavir (Figure 2). The instability of the P3 group is also reflected by the instability in the position of residue 8.

From our kinetic studies, it is clear that the nonactive-site mutations M46I and I54V provide for a high level of inhibitor resistance and cross resistance. Analyses of the regions containing the nonactive-site mutations found in our structures show regions of high variability when compared to the wild-type structures. The highest variability is seen in the 10's and 30's loops (Figure 3). The 30's loop contains the nonactive-site mutations L33F and M36I. The 10's loop contains the mutation K20R. Residue 20 is found juxtaposed to residues 33 and 36. The structural changes seen in these loops can be attributed to these mutations. A hydrogen-bonding network that is not present in the wild-type structure is established between the two strands (Figure 7). The Lys20 establishes hydrogen bonds with the carboxyl oxygen of residues Glu35 and Leu19 in both chains in both structures. Hydrogen bonds are found between the ϵ O and ϵ N of Gln18 and the amine and carboxyl oxygen, respectively, of Ser37 in both structures. The orientation of the ϵ O and ϵ NH₂ of

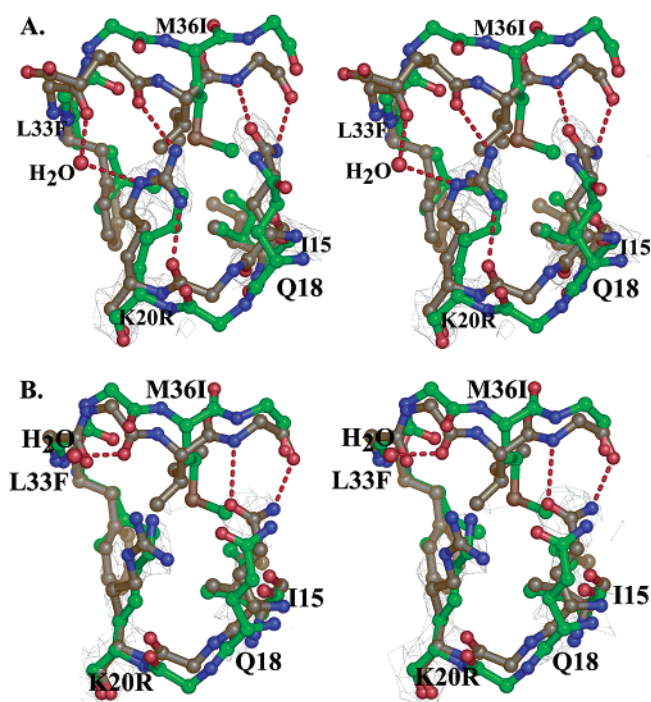


FIGURE 7: Stereoview of a C α overlap and hydrogen-bonding interactions between the 10's and 30's loops of chain A for the V6^{54/84}–indinavir (grey) and 1HSG (green) (A) and V6^{54/84}–ritonavir (grey) and 1HXW (green) (B). Residues 15, 18, 20, 33, and 36 are shown as ball-and-stick models. The electron densities for residues 18 and 20 are drawn to 2 σ and 1.5 σ for the V6^{54/84}–indinavir and V6^{54/84}–ritonavir, respectively.

Gln18 in both chains was based on the potential for hydrogen bonding.

We previously postulated the effects of mutations in this region to affect the dynamics of flap opening and closing (18). The presence of Phe33, Ileu25, and the α – α C of Lys20 form a highly hydrophobic pocket into which Ile36 fits, allowing the loops to come closer, an average of 2.9 and 3.1 Å for chain A and B, respectively, for both structures and allowing the formation of the hydrogen-bonding network discussed above. It is apparent that the structural changes found between the 30's loop and the 10's loops are pinching that region of the protease. A C α carbon overlap of the unbound (PDB 3HVP) and wild-type and V6^{54/84}-bound structures also show the greatest C α distance differences to map to the flaps (residues 45–55) and the 10's, 30's, and 80's loops (Figure 8). The presence of mutation I54V changes the interactions that occur between the flaps, the 80's loops, and the opposite flap. The M46I mutation, juxtaposed to residue 54, may function to stabilize the position of residue 54 by interacting with residues 53 and 55. The I84V along with mutations V82A and V32I further destabilizes the core of the inhibitor, which is also involved in two water-mediated hydrogen bonds with the flaps.

We postulate that the effects on inhibitor binding that we see because of the M46I, I54V, and I84V mutations are a result of changes in the interactions between the active-site residues and the inhibitor but, to a greater extent, are a result of changes in the opening and closing dynamics of the flaps caused by the nonactive-site mutations. Work done by other laboratories has shown that changes in the binding affinities of the inhibitors are due to a decrease of k_{on} and an increase

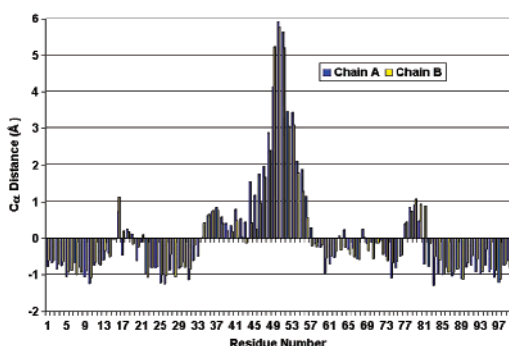
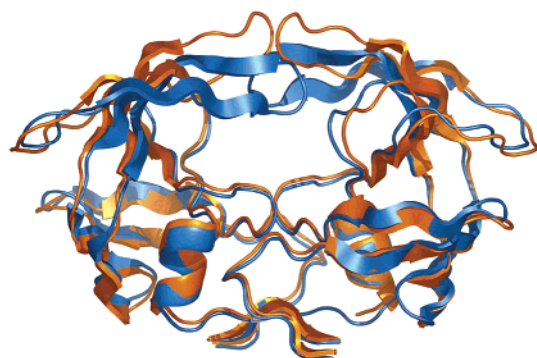


FIGURE 8: Ribbon representation of a C α overlap of PDB 1HSG and 3HVP. Below the overlap is a bar-graph representation of the C α distances between the structures for chain A (blue) and chain B (yellow). The graph was created by subtracting the average C α distance for each chain from the C α distance of each residue in the corresponding chain.

of k_{off} rates or an increase of k_{off} rates (52, 53). This would be consistent with an inability to form stable interactions with the flaps. We postulate that changes in the dynamics of the flaps opening and closing would have a greater effect on the stable binding of rigid inhibitors than the transient binding of flexible substrates. We propose that the interactions coordinated by residue 54 with the 80's loops, the opposite β strand of the flaps, and residue 50 of the opposite chain flap are altered by the M46I and I54V mutations and that along with structural changes in the 30's loops, when compared to the unbound structure, they function to destabilize the flaps promoting the open conformation of the protease.

After two decades of intense research around the world, HIV is still a major therapeutic challenge. New drugs for HIV targeting both reverse transcriptase and protease have given those living with the disease hope for the future. Still, therapy is life-long and laboring because of the ability of HIV to quickly acquire resistant mutations, leading to viruses that are cross-resistant to various protease inhibitors. With the presence of these mutations in therapy-naïve patients and in the transmission of HIV-1-resistant variants at the time of infection, it has also become clear that a better understanding of these variations is required for initial and ongoing treatment decisions (54–56). Our study shows that the accumulation of commonly seen resistant mutations to one inhibitor (ritonavir) will provide for a sufficiently catalytically active protease for virus viability, while providing a large degree of cross resistance. Structural analysis of the most resistance protease in this study shows large structural changes in and away from the active site, suggesting destabilization of the protease closed conformation. Although

our in vitro analysis is not without its limitations, it should prove useful in the design of new and continuing therapy.

ACKNOWLEDGMENT

We thank Dr. Alexander Wlodawer, Dr. Alla Gustchina, and Mi Li for their advice in crystallizing the HIV protease. We also thank the following for gifts of the HIV protease inhibitors: Abbott Laboratories (ritonavir), Agouron Pharmaceuticals, now Pfizer, San Diego, CA (nelfinavir and AG1776), and Merck (indinavir).

REFERENCES

- Velazquez-Campoy, A., Vega, S., and Freire, E. (2002) Amplification of the effects of drug resistance mutations by background polymorphisms in HIV-1 protease from African subtypes, *Biochemistry* 41, 8613–8619.
- Towler, E. M., Thompson, S. K., Tomaszek, T., and Debouck, C. (1997) Identification of a loop outside the active site cavity of the human immunodeficiency virus proteases which confers inhibitor specificity, *Biochemistry* 36, 5128–5133.
- Swairjo, M. A., Towler, E. M., Debouck, C., and Abdel-Meguid, S. S. (1998) Structural role of the 30's loop in determining the ligand specificity of the human immunodeficiency virus protease, *Biochemistry* 37, 10928–10936.
- Smidt, M. L., Potts, K. E., Tucker, S. P., Blystone, L., Stiebel, T. R., Jr., Stallings, W. C., McDonald, J. J., Pillay, D., Richman, D. D., and Bryant, M. L. (1997) A mutation in human immunodeficiency virus type 1 protease at position 88, located outside the active site, confers resistance to the hydroxyethylurea inhibitor SC-55389A, *Antimicrob. Agents Chemother.* 41, 515–522.
- Olsen, D. B., Stahlhut, M. W., Rutkowski, C. A., Schock, H. B., van Olden, A. L., and Kuo, L. C. (1999) Nonactive site changes elicit broad-based cross-resistance of the HIV-1 protease to inhibitors, *J. Biol. Chem.* 274, 23699–23701.
- Hoog, S. S., Towler, E. M., Zhao, B., Doyle, M. L., Debouck, C., and Abdel-Meguid, S. S. (1996) Human immunodeficiency virus protease ligand specificity conferred by residues outside of the active site cavity, *Biochemistry* 35, 10279–10286.
- Wlodawer, A., and Gustchina, A. (2000) Structural and biochemical studies of retroviral proteases, *Biochim. Biophys. Acta* 1477, 16–34.
- Tomasselli, A. G., and Heinrikson, R. L. (2000) Targeting the HIV-protease in AIDS therapy: A current clinical perspective, *Biochim. Biophys. Acta* 1477, 189–214.
- Dunn, B. M. (2002) Anatomy and pathology of HIV-1 peptidase, *Essays Biochem.* 38, 113–127.
- Molla, A., Korneyeva, M., Gao, Q., Vasavanonda, S., Schipper, P. J., Mo, H. M., Markowitz, M., Chernyavskiy, T., Niu, P., Lyons, N., Hsu, A., Granneman, G. R., Ho, D. D., Boucher, C. A., Leonard, J. M., Norbeck, D. W., and Kempf, D. J. (1996) Ordered accumulation of mutations in HIV protease confers resistance to ritonavir, *Nat. Med.* 2, 760–766.
- Para, M. F., Glidden, D. V., Coombs, R. W., Collier, A. C., Condra, J. H., Craig, C., Bassett, R., Leavitt, R., Snyder, S., McAuliffe, V., and Boucher, C. (2000) Baseline human immunodeficiency virus type 1 phenotype, genotype, and RNA response after switching from long-term hard-capsule saquinavir to indinavir or soft-gel-capsule saquinavir in AIDS clinical trials group protocol 333, *J. Infect. Dis.* 182, 733–743.
- Zolopa, A. R., Shafer, R. W., Warford, A., Montoya, J. G., Hsu, P., Katzenstein, D., Merigan, T. C., and Efron, B. (1999) HIV-1 genotypic resistance patterns predict response to saquinavir-ritonavir therapy in patients in whom previous protease inhibitor therapy had failed, *Ann. Intern. Med.* 131, 813–821.
- Condra, J. H., Petropoulos, C. J., Ziermann, R., Schleif, W. A., Shivaprakash, M., and Emini, E. A. (2000) Drug resistance and predicted virologic responses to human immunodeficiency virus type 1 protease inhibitor therapy, *J. Infect. Dis.* 182, 758–765.
- Patick, A. K., Duran, M., Cao, Y., Shugarts, D., Keller, M. R., Mazabel, E., Knowles, M., Chapman, S., Kuritzkes, D. R., and Markowitz, M. (1998) Genotypic and phenotypic characterization of human immunodeficiency virus type 1 variants isolated from patients treated with the protease inhibitor nelfinavir, *Antimicrob. Agents Chemother.* 42, 2637–2644.

15. Ido, E., Han, H. P., Kezdy, F. J., and Tang, J. (1991) Kinetic studies of human immunodeficiency virus type 1 protease and its active-site hydrogen bond mutant A28S, *J. Biol. Chem.* 266, 24359–24366.
16. Goodenow, M. M., Bloom, G., Rose, S. L., Pomeroy, S. M., O'Brien, P. O., Perez, E. E., Sleasman, J. W., and Dunn, B. M. (2002) Naturally occurring amino acid polymorphisms in human immunodeficiency virus type 1 (HIV-1) Gag p7(NC) and the C-cleavage site impact Gag-Pol processing by HIV-1 protease, *Virology* 292, 137–149.
17. Wain-Hobson, S., Sonigo, P., Danos, O., Cole, S., and Alizon, M. (1985) Nucleotide sequence of the AIDS virus, LAV, *Cell* 40, 9–17.
18. Clemente, J. C., Hemrajani, R., Blum, L. E., Goodenow, M. M., and Dunn, B. M. (2003) Secondary mutations M36I and A71V in the human immunodeficiency virus type 1 protease can provide an advantage for the emergence of the primary mutation D30N, *Biochemistry* 42, 15029–15035.
19. Dunn, B. M., Gustchina, A., Wlodawer, A., and Kay, J. (1994) Subsite preferences of retroviral proteinases, *Methods Enzymol.* 241, 254–278.
20. Bhatt, D., and Dunn, B. M. (2000) Chimeric aspartic proteinases and active site binding, *Bioorg. Chem.* 28, 374–393.
21. Otwinowski, Z., and Minor, W. (1997) in *Macromolecular Crystallography, Part A*, pp 307–326.
22. Brunger, A. T., Adams, P. D., Clore, G. M., DeLano, W. L., Gros, P., Grosse-Kunstleve, R. W., Jiang, J. S., Kuszewski, J., Nilges, M., Pannu, N. S., Read, R. J., Rice, L. M., Simonson, T., and Warren, G. L. (1998) Crystallography and NMR system: A new software suite for macromolecular structure determination, *Acta Crystallogr., Sect. D* 54 (Part 5), 905–921.
23. Jones, T. A., Zou, J. Y., Cowan, S. W., and Kjeldgaard, M. (1991) Improved methods for building protein models in electron-density maps and the location of errors in these models, *Acta Crystallogr., Sect. A* 47, 110–119.
24. DeLano, W. L. (2002) DeLano Scientific, San Carlos, CA.
25. Keil, M., Exner, T., and Brickmann, J. (1998) Characterisation of protein–ligand interfaces: Separating surfaces, *J. Mol. Model.* 4, 335–339.
26. Exner, T., Keil, M., Moeckel, G., and Brickmann, J. (1998) Identification of substrate channels and protein cavities, *J. Mol. Model.* 4, 340–343.
27. Lin, Y., Lin, X., Hong, L., Foundling, S., Heinrikson, R. L., Thaisrivongs, S., Leelamanit, W., Rateman, D., Shah, M., Dunn, B. M., and et al. (1995) Effect of point mutations on the kinetics and the inhibition of human immunodeficiency virus type 1 protease: Relationship to drug resistance, *Biochemistry* 34, 1143–1152.
28. Muzammil, S., Ross, P., and Freire, E. (2003) A major role for a set of non-active site mutations in the development of HIV-1 protease drug resistance, *Biochemistry* 42, 631–638.
29. Wilson, S. I., Phylip, L. H., Mills, J. S., Gulnik, S. V., Erickson, J. W., Dunn, B. M., and Kay, J. (1997) Escape mutants of HIV-1 proteinase: Enzymic efficiency and susceptibility to inhibition, *Biochim. Biophys. Acta* 1339, 113–125.
30. Condra, J. H., Holder, D. J., Schleif, W. A., Blahy, O. M., Danovich, R. M., Gabryelski, L. J., Graham, D. J., Laird, D., Quintero, J. C., Rhodes, A., Robbins, H. L., Roth, E., Shivaprakash, M., Yang, T., Chodakewitz, J. A., Deutsch, P. J., Leavitt, R. Y., Massari, F. E., Mellors, J. W., Squires, K. E., Steigbigel, R. T., Teppler, H., and Emini, E. A. (1996) Genetic correlates of in vivo viral resistance to indinavir, a human immunodeficiency virus type 1 protease inhibitor, *J. Virol.* 70, 8270–8276.
31. Dronda, F., Casado, J. L., Moreno, S., Hertogs, K., Garcia-Arata, I., Antela, A., Perez-Elias, M. J., Ruiz, L., and Larder, B. (2001) Phenotypic cross-resistance to nelfinavir: The role of prior antiretroviral therapy and the number of mutations in the protease gene, *AIDS Res. Hum. Retroviruses* 17, 211–215.
32. Hertogs, K., Bloor, S., De Vroey, V., van Den Eynde, C., Dehertogh, P., van Cauwenberge, A., Sturmer, M., Alcorn, T., Wegner, S., van Houtte, M., Miller, V., and Larder, B. A. (2000) A novel human immunodeficiency virus type 1 reverse transcriptase mutational pattern confers phenotypic lamivudine resistance in the absence of mutation 184V, *Antimicrob. Agents Chemother.* 44, 568–573.
33. Lawrence, J., Schapiro, J., Winters, M., Montoya, J., Zolopa, A., Pesano, R., Efron, B., Winslow, D., and Merigan, T. C. (1999) Clinical resistance patterns and responses to two sequential protease inhibitor regimens in saquinavir and reverse transcriptase inhibitor-experienced persons, *J. Infect. Dis.* 179, 1356–1364.
34. Wiegers, K., Rutter, G., Kottler, H., Tessmer, U., Hohenberg, H., and Krausslich, H. G. (1998) Sequential steps in human immunodeficiency virus particle maturation revealed by alterations of individual Gag polyprotein cleavage sites, *J. Virol.* 72, 2846–2854.
35. Pettit, S. C., Moody, M. D., Wehbie, R. S., Kaplan, A. H., Nantermet, P. V., Klein, C. A., and Swanstrom, R. (1994) The p2 domain of human immunodeficiency virus type 1 Gag regulates sequential proteolytic processing and is required to produce fully infectious virions, *J. Virol.* 68, 8017–8027.
36. Chen, E. (1994) Host strain selection for bacterial expression of toxic proteins, *Methods Enzymol.* 241, 29–46.
37. Deeks, S. G., Grant, R. M., Beatty, G. W., Horton, C., Detmer, J., and Eastman, S. (1998) Activity of a ritonavir plus saquinavir-containing regimen in patients with virologic evidence of indinavir or ritonavir failure, *AIDS* 12, F97–F102.
38. Karmochkine, M., Si Mohamed, A., Piketty, C., Ginsburg, C., Raguin, G., Schneider-Fauveau, V., Gutmann, L., Kazatchkine, M. D., and Belec, L. (2000) The cumulative occurrence of resistance mutations in the HIV-1 protease gene is associated with failure of salvage therapy with ritonavir and saquinavir in protease inhibitor-experienced patients, *Antiviral. Res.* 47, 179–188.
39. Pazhanisamy, S., Stuver, C. M., Cullinan, A. B., Margolin, N., Rao, B. G., and Livingston, D. J. (1996) Kinetic characterization of human immunodeficiency virus type-1 protease-resistant variants, *J. Biol. Chem.* 271, 17979–17985.
40. Yoshimura, K., Kato, R., Yusa, K., Kavlick, M. F., Maroun, V., Nguyen, A., Mimoto, T., Ueno, T., Shintani, M., Falloon, J., Masur, H., Hayashi, H., Erickson, J., and Mitsuya, H. (1999) JE-2147: A dipeptide protease inhibitor (PI) that potently inhibits multi-PI-resistant HIV-1, *Proc. Natl. Acad. Sci. U.S.A.* 96, 8675–8680.
41. Gatanaga, H., Suzuki, Y., Tsang, H., Yoshimura, K., Kavlick, M. F., Nagashima, K., Gorelick, R. J., Mardy, S., Tang, C., Summers, M. F., and Mitsuya, H. (2002) Amino acid substitutions in Gag protein at noncleavage sites are indispensable for the development of a high multitude of HIV-1 resistance against protease inhibitors, *J. Biol. Chem.* 277, 5952–5961.
42. Johnson, V. A., Brun-Vézinet, F., Clotet, B., Conway, B., D'Aquila, R. T., Demeter, L. M., Kuritzkes, D. R., Pillay, D., Schapiro, J. M., Telenti, A., and Richman, D. D. (2003) Drug resistance mutations in HIV-1, *Top. HIV Med.* 11, 215–221.
43. Hoffman, N. G., Schiffer, C. A., and Swanstrom, R. (2003) Covariation of amino acid positions in HIV-1 protease, *Virology* 314, 536–548.
44. Ohtaka, H., Schon, A., and Freire, E. (2003) Multidrug resistance to HIV-1 protease inhibition requires cooperative coupling between distal mutations, *Biochemistry* 42, 13659–13666.
45. Munshi, S., Chen, Z., Yan, Y., Li, Y., Olsen, D. B., Schock, H. B., Galvin, B. B., Dorsey, B., and Kuo, L. C. (2000) An alternate binding site for the P1–P3 group of a class of potent HIV-1 protease inhibitors as a result of concerted structural change in the 80s loop of the protease, *Acta. Crystallogr., Sect. D* 56 (Part 4), 381–388.
46. Babe, L. M., Rose, J., and Craik, C. S. (1995) Trans-dominant inhibitory human immunodeficiency virus type 1 protease monomers prevent protease activation and virion maturation, *Proc. Natl. Acad. Sci. U.S.A.* 92, 10069–10073.
47. McPhee, F., Good, A. C., Kuntz, I. D., and Craik, C. S. (1996) Engineering human immunodeficiency virus 1 protease heterodimers as macromolecular inhibitors of viral maturation, *Proc. Natl. Acad. Sci. U.S.A.* 93, 11477–11481.
48. Gulnik, S. V., Suvorov, L. I., Liu, B., Yu, B., Anderson, B., Mitsuya, H., and Erickson, J. W. (1995) Kinetic characterization and cross-resistance patterns of HIV-1 protease mutants selected under drug pressure, *Biochemistry* 34, 9282–9287.
49. Vega, S., Kang, L. W., Velazquez-Campoy, A., Kiso, Y., Amzel, L. M., and Freire, E. (2004) A structural and thermodynamic escape mechanism from a drug resistant mutation of the HIV-1 protease, *Proteins* 55, 594–602.
50. Swairjo, M. A., Towler, E. M., Debouck, C., and Abdel-Meguid, S. S. (1998) Structural role of the 30's loop in determining the ligand specificity of the human immunodeficiency virus protease, *Biochemistry* 37, 10928–10936.

51. Stebbins, J., Towler, E. M., Tennant, M. G., Deckman, I. C., and Debouck, C. (1997) The 80's loop (residues 78–85) is important for the differential activity of retroviral proteases, *J. Mol. Biol.* 267, 467–475.
52. Maschera, B., Darby, G., Palu, G., Wright, L. L., Tisdale, M., Myers, R., Blair, E. D., and Furfine, E. S. (1996) Human immunodeficiency virus. Mutations in the viral protease that confer resistance to saquinavir increase the dissociation rate constant of the protease-saquinavir complex, *J. Biol. Chem.* 271, 33231–33235.
53. Shuman, C. F., Markgren, P. O., Hamalainen, M., and Danielson, U. H. (2003) Elucidation of HIV-1 protease resistance by characterization of interaction kinetics between inhibitors and enzyme variants, *Antiviral Res.* 58, 235–242.
54. Frater, A. J., Beardall, A., Ariyoshi, K., Churchill, D., Galpin, S., Clarke, J. R., Weber, J. N., and McClure, M. O. (2001) Impact of baseline polymorphisms in RT and protease on outcome of highly active antiretroviral therapy in HIV-1-infected African patients, *AIDS* 15, 1493–1502.
55. Perno, C. F., Cozzi-Lepri, A., Balotta, C., Forbici, F., Violin, M., Bertoli, A., Facchi, G., Pezzotti, P., Cadeo, G., Tositti, G., Pasquinucci, S., Pauluzzi, S., Scalzini, A., Salassa, B., Vincenti, A., Phillips, A. N., Dianzani, F., Appice, A., Angarano, G., Monno, L., Ippolito, G., Moroni, M., and d' Arminio Monforte, A. (2001) Secondary mutations in the protease region of human immunodeficiency virus and virologic failure in drug-naïve patients treated with protease inhibitor-based therapy, *J. Infect. Dis.* 184, 983–991.
56. Palmer, S., Alaeus, A., Albert, J., and Cox, S. (1998) Drug susceptibility of subtypes A, B, C, D, and E human immunodeficiency virus type 1 primary isolates, *AIDS Res. Hum. Retroviruses* 14, 157–162.
57. Wallace, A. C., Laskowski, R. A., and Thornton, J. M. (1995) LIGPLOT: A program to generate schematic diagrams of protein–ligand interactions, *Protein Eng.* 8, 127–134.

BI049459M